

On the role of dynamic electron correlation in
non-orthogonal configuration interaction with fragments
Supplementary information

A. Sánchez-Mansilla,^a C. Sousa,^b R. K. Kathir,^c

R. Broer,^c T. P. Straatsma,^{d,e} and C. de Graaf^{*a,c,f}

(a) Departament de Química Física i Inorgànica

Universitat Rovira i Virgili, Tarragona, Spain.

(b) Departament de Química Física and Institut de Química

Teòrica i Computacional, Universitat de Barcelona, Spain

(c) Zernike Institute of Advanced Materials

University of Groningen, Netherlands

(d) National Center for Computational Sciences, Oak Ridge

National Laboratory, Oak Ridge, TN 37831-6373, U. S. A.

(e) Department of Chemistry and Biochemistry,

University of Alabama, Tuscaloosa, AL 35487-0336, U. S. A.

(f) ICREA, Pg. Lluís Companys 23, Barcelona, Spain

E-mail: csousa@ub.edu, coen.degraaf@urv.cat

May 2, 2022

1 Shifting the diagonal matrix elements: orthogonal versus non-orthogonal basis

The effect of shifting the diagonal matrix elements is illustrated in a 2×2 example. The secular equations read

$$\begin{pmatrix} H_{11} - ES_{11} & H_{21} - ES_{21} \\ H_{12} - ES_{12} & H_{22} - ES_{22} \end{pmatrix} \begin{pmatrix} c_1 \\ c_2 \end{pmatrix} = \begin{pmatrix} 0 \\ 0 \end{pmatrix} \quad (1)$$

and with $S_{12} = S_{21} = S$, $S_{11} = S_{22} = 1$, and $H_{12} = H_{21} = V$, the solutions are

$$E_{\pm} = \frac{-(2VS - H_{11} - H_{22}) \pm \sqrt{(2VS - H_{11} - H_{22})^2 - 4(1 - S^2)(H_{11}H_{22} - V^2)}}{2(1 - S^2)} \quad (2)$$

By shifting H_{11} to $H_{11} + \alpha$, the energy difference becomes

$$E_+ - E_- = \frac{\sqrt{(2VS - H_{11} - \alpha - H_{22})^2 - 4(1 - S^2)((H_{11} + \alpha)H_{22} - V^2)}}{1 - S^2} \quad (3)$$

which reduces to

$$E_+ - E_- = \sqrt{\alpha^2 + 2\alpha(H_{11} - H_{22}) + (H_{11} - H_{22})^2 + 4V^2} \quad (4)$$

when H is expressed in an orthogonal basis, that is $S = 0$. This shows that $\Delta E = E_+ - E_-$ depends on the values of the diagonal matrix elements when the shift is applied in the non-orthogonal basis, that is, on the choice of the zero of energy, while it only depends on the difference of these elements when an orthogonal basis is used.

As numerical example, substituting $H_{11} = 1$, $H_{22} = 2$, $\alpha = 0.2$, and $V = 0.1$ leads to $\Delta E = 0.8246$ for $S = 0$ and $\Delta E = 0.8131$ for $S = 0.1$. This energy difference remains the same in the non-overlapping case when H_{11} and H_{22} are changed to 2 and 3, but becomes 0.8666 for the non-orthogonal basis. Hence, shifting the diagonal matrix elements with a dynamic correlation energy correction can only be done after transforming the NOCI hamiltonian to a basis of orthogonal MEBFs.

2 Electronic coupling in singlet fission: tetracene

CASSCF(8,8) and CASPT2 calculations were performed with OpenMolcas,¹ the CASSCF(6,6), DCD-CAS(2) and NEVPT2 calculations with Orca 4.2.² ANO-RCC basis sets were used in the OpenMolcas calculations (4s,3p,1d and 3s,1p contractions for C and H, respectively), def2-TZVP basis sets in Orca. The standard CASPT2 IPEA=0.25 zeroth order Hamiltonian was used and an imaginary level shift of 0.15 was applied to avoid intruder states. CASPT2 and NEVPT2 correlate all electrons, except the C- $1s^2$ core electrons. The threshold for the construction of the common MO basis was 10^{-5} .

For the direct coupling we construct two new MEBFs from the S0S1 and S1S0 MEBFs by diagonalizing the S0S1, S1S0 block of the NOCI matrix and select the eigenfunctions as new, (partly) delocalized MEBFs. These new MEBFs and the 1TT MEBF are then used to construct the corresponding 3x3 H and S matrices. The matrix elements of these matrices are then substituted in Eq. 13 to calculate the electronic coupling. For the CT enhanced coupling we first diagonalize the S0S1, S1S0, D+D-, D-D+ block and select the eigenfunctions dominated by the S0S1, S1S0 MEBFs as new MEBFs. Then we diagonalize the 1TT, D+D-, D-D+ block and select the eigenvector with largest contribution from 1TT. These new 'dressed' MEBFs are used to construct the corresponding 3x3 H and S matrices and to compute the electronic coupling in the same way as for the direct coupling. For the CT enhanced coupling with DCEC, the shifted hamiltonian is used to built the *dressed* MEBFs. With this way of addressing the two mechanisms, the CT enhanced coupling does also include the direct coupling. In all cases, we only report the largest coupling between the 1TT and S_0S_1 / S_1S_0 (dressed) combinations.

Table S1: Cartesian coordinates (in Å) of the three tetracence molecules considered in the calculations as extracted from the experimental crystal structure

Atom	<i>x</i>	<i>y</i>	<i>z</i>
fragment A			
C	-2.490662	-2.630368	-4.643162
C	-2.496492	-3.519246	-3.592412
C	-3.138058	-3.123730	-2.387176
C	-3.209826	-3.998475	-1.284931
C	-3.875230	-3.683889	-0.063756
C	-4.362783	-1.486587	-1.020098
C	-3.725544	-1.819151	-2.220429
C	-3.650554	-0.986912	-3.292023
C	-3.045415	-1.272278	-4.469059
C	-5.798468	-3.387063	4.643162
C	-5.792638	-2.498185	3.592412
C	-5.151072	-2.893702	2.387176
C	-5.079304	-2.018956	1.284931
C	-4.413900	-2.333542	0.063756
C	-3.926347	-4.530844	1.020098
C	-4.563585	-4.198281	2.220429
C	-4.638575	-5.030519	3.292023
C	-5.243715	-4.745153	4.469059
H	-2.027999	-2.967206	-5.566400
H	-2.063378	-4.492583	-3.739542
H	-2.780319	-4.998094	-1.397730
H	-4.787309	-0.530241	-0.882777
H	-4.097634	-0.009420	-3.101980
H	-3.004961	-0.596471	-5.210837
H	-6.261131	-3.050225	5.566400

–Continued on next page–

Table S1 – continued

Atom	<i>x</i>	<i>y</i>	<i>z</i>
H	-6.225752	-1.524848	3.739542
H	-5.508811	-1.019337	1.397730
H	-3.501821	-5.487190	0.882777
H	-4.191496	-6.008011	3.101980
H	-5.284168	-5.420960	5.210837
fragment B			
C	-2.101532	3.387063	-4.643162
C	-2.107362	2.498185	-3.592412
C	-2.748928	2.893702	-2.387176
C	-2.820696	2.018956	-1.284931
C	-3.486100	2.333542	-0.063756
C	-3.973653	4.530844	-1.020098
C	-3.336415	4.198281	-2.220429
C	-3.261425	5.030519	-3.292023
C	-2.656285	4.745153	-4.469059
C	-5.409338	2.630368	4.643162
C	-5.403508	3.519246	3.592412
C	-4.761942	3.123730	2.387176
C	-4.690174	3.998475	1.284931
C	-4.024770	3.683889	0.063756
C	-3.537217	1.486587	1.020098
C	-4.174456	1.819151	2.220429
C	-4.249446	0.986912	3.292023
C	-4.854585	1.272278	4.469059
H	-1.638869	3.050225	-5.566400
H	-1.674248	1.524848	-3.739542
H	-2.391189	1.019337	-1.397730
H	-4.398179	5.487190	-0.882777

–Continued on next page–

Table S1 – continued

Atom	<i>x</i>	<i>y</i>	<i>z</i>
H	-3.708504	6.008011	-3.101980
H	-2.615832	5.420960	-5.210837
H	-5.872001	2.967206	5.566400
H	-5.836622	4.492583	3.739542
H	-5.119681	4.998094	1.397730
H	-3.112691	0.530241	0.882777
H	-3.802366	0.009420	3.101980
H	-4.895039	0.596471	5.210837
fragment C			
C	1.117243	0.609775	-4.769448
C	0.474618	-0.271713	-3.946749
C	0.418464	-0.011430	-2.501202
C	-0.213271	-0.859889	-1.667468
C	-0.298843	-0.611419	-0.258703
C	-0.907618	-1.447989	0.632657
C	-0.954849	-1.185875	2.007092
C	-1.656807	-2.081951	2.887417
C	1.716809	1.826707	-4.270434
C	-1.716809	-1.826707	4.270434
C	0.907618	1.447989	-0.632657
C	0.954849	1.185875	-2.007092
C	1.656807	2.081951	-2.887417
C	-1.117243	-0.609775	4.769448
C	-0.474618	0.271713	3.946749
C	-0.418464	0.011430	2.501202
C	0.213271	0.859889	1.667468
C	0.298843	0.611419	0.258703
H	1.139003	0.375654	-5.762572

–Continued on next page–

Table S1 – continued

Atom	<i>x</i>	<i>y</i>	<i>z</i>
H	0.062028	-1.181756	-4.279017
H	-0.648696	-1.787042	-2.023031
H	-1.326843	-2.380514	0.269737
H	-1.992547	-2.977481	2.476680
H	2.153681	2.510691	-4.904317
H	-2.153681	-2.510691	4.904317
H	1.326843	2.380514	-0.269737
H	1.992547	2.977481	-2.476680
H	-1.139003	-0.375654	5.762572
H	-0.062028	1.181756	4.279017
H	0.648696	1.787042	2.023031

Table S2: CASSCF(6,6), CASPT2, NEVPT2 and DCD-CAS(2) relative energies (in eV) of the fragment wave functions used to construct the MEBFs of the tetracene dimers.

Fragment	State	CASSCF(6,6)	CASPT2	NEVPT2	DCD-CAS(2)
A/B	S_0	0.00	0.00	0.00	0.00
	S_1	4.24	2.73	2.32	2.44
	T_1	1.46	1.72	1.81	1.65
	D^+	6.18	6.85	6.75	6.73
	D^-	0.70	-0.88	-1.01	-1.03
C	S_0	0.00	0.00	0.00	0.00
	S_1	4.40	2.85	2.49	2.58
	T_1	1.81	1.87	1.99	1.82
	D^+	6.26	6.94	6.87	6.85
	D^-	0.78	-0.77	-0.85	-0.90

Table S3: Comparison of the direct and total electronic coupling (in meV) between 1TT and S_0S_1/S_1S_0 for the AB, AC and BC tetracene dimers with one-MEBF DCEC and GN-weighted DCEC.

dimer	one-MEBF DCEC		GN-weighted DCEC	
	direct	total	direct	total
AB	0.02	0.06	0.02	0.07
AC	0.38	8.37	0.38	8.36
BC	1.11	21.59	1.11	21.60

Table S4: Gallup-Norbeck weights of the original non-orthogonal MEBFs in the orthogonalized MEBFs Φ_i

MEBFs	orthogonalized MEBFs					
	Φ_1	Φ_2	Φ_3	Φ_4	Φ_5	Φ_6
S_0S_0	0.99982945	0.00003581	0.00009641	0.00000000	0.00002071	0.00001762
S_0S_1	0.00003583	0.99996099	0.00000002	0.00000000	0.00000220	0.00000095
S_1S_0	0.00009643	0.00000002	0.99989433	0.00000000	0.00000003	0.00000919
1TT	0.00000000	0.00000000	0.00000000	0.99997943	0.00001530	0.00000527
D^+D^-	0.00002072	0.00000220	0.00000003	0.00001530	0.99996174	0.00000000
D^-D^+	0.00001763	0.00000094	0.00000919	0.00000527	0.00000000	0.99996696

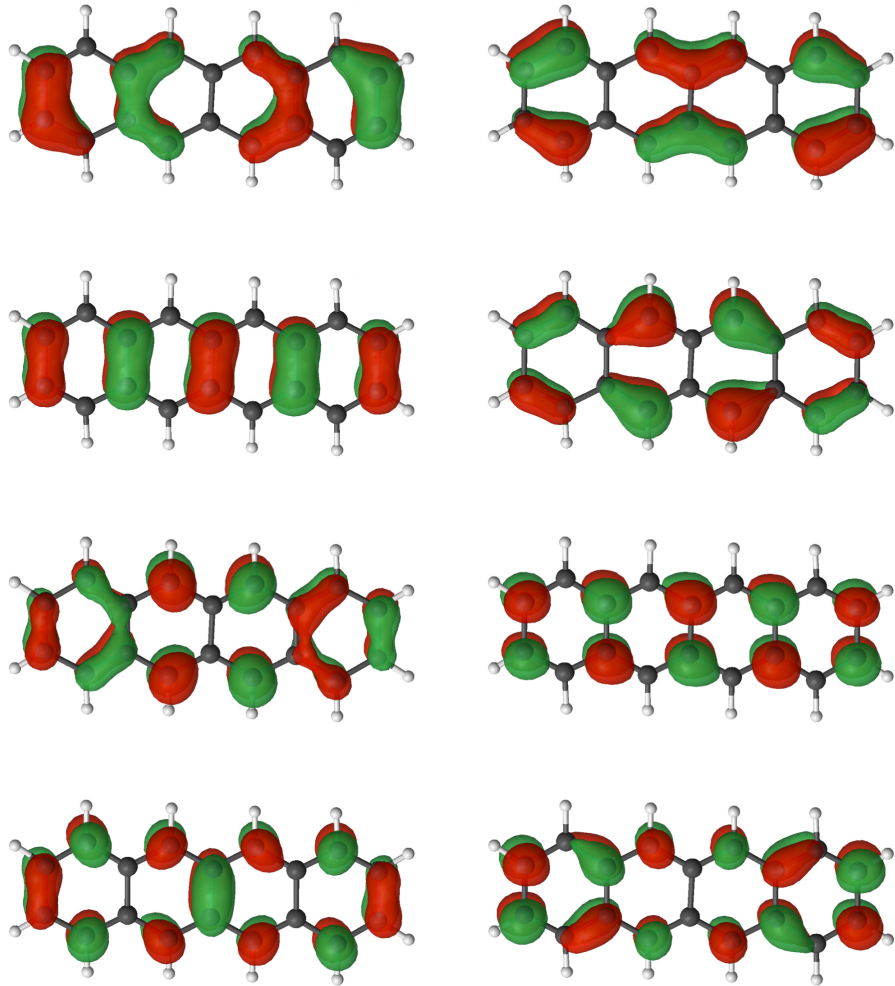


Figure S1: CASSCF(8,8) active orbitals of the S_0 state of fragment A. Active orbitals of all other states in all three fragments are slightly different but have similar shape.

Table S5: Weights of the most important electronic configurations in the CASSCF(6,6) and DCD-CAS(2) wave function of the A, B and C fragment wave functions. The electronic configuration is given by the occupation number of the six active orbitals.

State	conf.	Fragment A/B		Fragment C	
		CAS(6,6)	DCD-CAS(2)	CAS(6,6)	DCD-CAS(2)
S_0	2 2 2 0 0 0	0.872	0.929	0.889	0.936
	2 2 0 2 0 0	0.042	0.026	0.031	0.020
	2 1 1 1 1 0	0.032	0.017	0.027	0.015
	1 2 1 1 0 1	0.014	0.007	0.014	0.007
	1 1 2 0 1 1	0.011	0.005	0.011	0.005
	0 2 2 0 0 2	0.007	0.003	0.008	0.004
	Total	0.983	0.989	0.980	0.987
S_1	2 2 1 1 0 0	0.933	0.954	0.935	0.956
	2 1 2 0 1 0	0.009	0.006	0.010	0.006
	1 1 2 2 0 0	0.009	0.007	0.008	0.006
	1 1 1 1 1 1	0.009	0.004	0.008	0.004
	1 2 1 1 1 0	0.007	0.005	0.007	0.004
	Total	0.967	0.976	0.968	0.976
T_1	2 2 1 1 0 0	0.874	0.946	0.880	0.947
	2 1 2 0 1 0	0.033	0.016	0.034	0.017
	1 2 1 1 1 0	0.020	0.008	0.017	0.007
	2 1 1 1 0 1	0.017	0.007	0.015	0.006
	1 1 1 1 1 1	0.016	0.006	0.015	0.006
	2 1 0 2 1 0	0.012	0.005	0.010	0.005
	Total	0.972	0.988	0.971	0.988

–Continued on next page–

TABLE S5 – continued

State	conf.	Fragment A/B		Fragment C	
		CAS(6,6)	DCD-CAS(2)	CAS(6,6)	DCD-CAS(2)
D^+	2 2 1 0 0 0	0.922	0.961	0.926	0.962
	1 1 2 1 0 0	0.007	0.003	0.006	0.003
	2 1 0 1 1 0	0.007	0.004	0.005	0.003
	2 1 1 0 0 1	0.006	0.003	0.004	0.003
	2 0 1 2 0 0	0.006	0.003	0.005	0.003
	1 1 1 0 1 1	0.006	0.003	0.009	0.004
	Total	0.954	0.977	0.955	0.978
D^-	2 2 2 1 0 0	0.934	0.961	0.937	0.961
	2 1 1 1 1 1	0.010	0.004	0.010	0.005
	1 1 2 2 1 0	0.007	0.004	0.006	0.004
	2 2 1 1 1 0	0.007	0.003	0.006	0.003
	1 2 1 2 0 1	0.006	0.003	0.006	0.003
	Total	0.964	0.975	0.965	0.976

Table S6: Relative energies (in eV) of the fragment wave functions of the benzene dimer

State	CASSCF(6,6)	CASPT2	DCD-CAS
S_0	0.0	0.0	0.0
S_1	5.1	5.3	5.3
T_1	4.0	4.4	4.4
D^+	8.4	9.3	9.3
D^-	3.3	1.7	1.8

Table S7: Electronic coupling (in meV) between the S_0S_1 and 1TT MEBFs in the benzene dimer as function of the intermolecular distance (in Å)

distance	CASSCF(6,6)	DCD-CAS	DCD-CAS + DCEC
3.00	15.97	16.39	16.33
3.25	8.65	9.03	9.00
3.50	4.54	4.82	4.80
3.75	2.31	2.49	2.48

3 Wave function analysis: diazadiborinine derivative

Optimization of the periodic structure of the diazadiborinine derivative was performed with the Crystal17 code.³ DFT/B3LYP extended with Grimme's D3 dispersion corrections⁴ were used to calculate the electronic structure and minimize the energy with respect to the atomic positions and the lattice parameters under the restriction of the space group of the parent compound.⁵ A Gaussian type atom-centered basis set was used of triple zeta + polarization quality⁶ for all atoms in the unit cell. A 4x4x4 Monkhorst-Pack lattice of k-points was used.^{7,8} All other computational parameters such as the ones that control the truncation of the two-electron integrals and the energy and geometry convergence were kept at their default values. The optimized geometry is specified in Table S8.

Table S8: Optimized lattice parameters and atomic positions of the diazadiborinine derivative.
 Lattice parameters: $a = 25.95066 \text{ \AA}$; $b = 8.3992 \text{ \AA}$; $c = 11.8842 \text{ \AA}$; $\beta = 116.98$

Atom	x/a	y/b	z/c
N	-0.0163	-0.1590	0.4640
N	-0.0714	-0.1153	0.2573
N	-0.2625	-0.0893	-0.0312
N	-0.2110	-0.0562	-0.1386
B	0.2099	0.3416	0.0405
B	0.0227	-0.1345	-0.4023
C	-0.2665	0.0710	-0.0692
C	-0.2265	-0.1709	-0.0731
C	-0.2344	0.0894	-0.1330
C	-0.1741	-0.0802	-0.2002
C	0.1670	0.4501	0.0688
C	-0.0371	-0.0376	0.3714
C	-0.0395	-0.3053	0.4042
C	-0.0727	-0.2769	0.2784
C	-0.0959	-0.0417	0.1326

–Continued on next page–

TABLE S8 – continued

Atom	x/a	y/b	z/c
C	0.0473	-0.2852	-0.3130
H	0.2083	-0.3432	-0.0477
H	-0.2271	0.1929	-0.1781
H	-0.1816	0.0184	-0.2660
H	-0.1851	-0.1922	-0.2527
H	-0.1281	-0.0826	-0.1321
H	-0.0319	-0.4148	0.4566
H	-0.0975	-0.3581	0.2022
H	-0.1142	-0.1362	0.0628
H	-0.0618	0.0202	0.1192
H	-0.1305	0.0424	0.1197
H	0.1894	-0.4561	0.1390
H	0.1356	-0.4875	-0.0167
H	0.1415	0.3832	0.1051
H	0.0679	-0.2560	-0.2121
H	0.0136	-0.3738	-0.3273
H	0.0800	-0.3481	-0.3314

Table S9: CASSCF(8,8) and CASPT2 relative energies (in eV) of the A, B and C fragments used to construct the MEBFs of the diazadiborinine derivative

State	A and C		B	
	CASSCF(8,8)	CASPT2	CASSCF(8,8)	CASPT2
S_0	0.00	0.00	0.00	0.00
S_1	3.69	3.63	3.74	3.69
T_1	1.23	1.92	1.33	1.92
D^+	4.38	4.80	4.19	4.95
D^-	2.27	1.10	2.30	1.13

Table S10: MEBF relative energies (in eV) of the AB, AC and BC dimers before and after applying the dynamic correlation energy correction (DCEC)

MEBF	AB		AC		BC	
	no DCEC	DCEC	no DCEC	DCEC	no DCEC	DCEC
S_0S_0	0.00	0.00	0.00	0.00	0.00	0.00
S_1S_0	3.81	3.75	3.70	3.65	3.70	3.65
S_0S_1	3.82	3.76	3.64	3.58	3.66	3.60
T_1T_1	2.55	3.92	2.43	3.70	2.44	3.71
D^+D^-	4.61	3.87	5.46	4.71	4.97	4.22
D^-D^+	4.61	3.87	5.05	4.64	4.38	3.97

Table S11: Relative energies (in eV) of the NOCI states of the AB, AC and BC dimers before and after applying the dynamic correlation energy correction (DCEC)

State	AB		AC		BC	
	no DCEC	DCEC	no DCEC	DCEC	no DCEC	DCEC
Ψ_0	0.00	0.00	0.00	0.00	0.00	0.00
Ψ_1	2.54	3.67	2.43	3.58	2.44	3.59
Ψ_2	3.79	3.70	3.64	3.65	3.65	3.65
Ψ_3	3.84	3.78	3.70	3.70	3.70	3.69
Ψ_4	4.65	3.97	5.05	4.64	4.39	4.00
Ψ_5	4.68	4.17	5.47	4.72	4.98	4.24

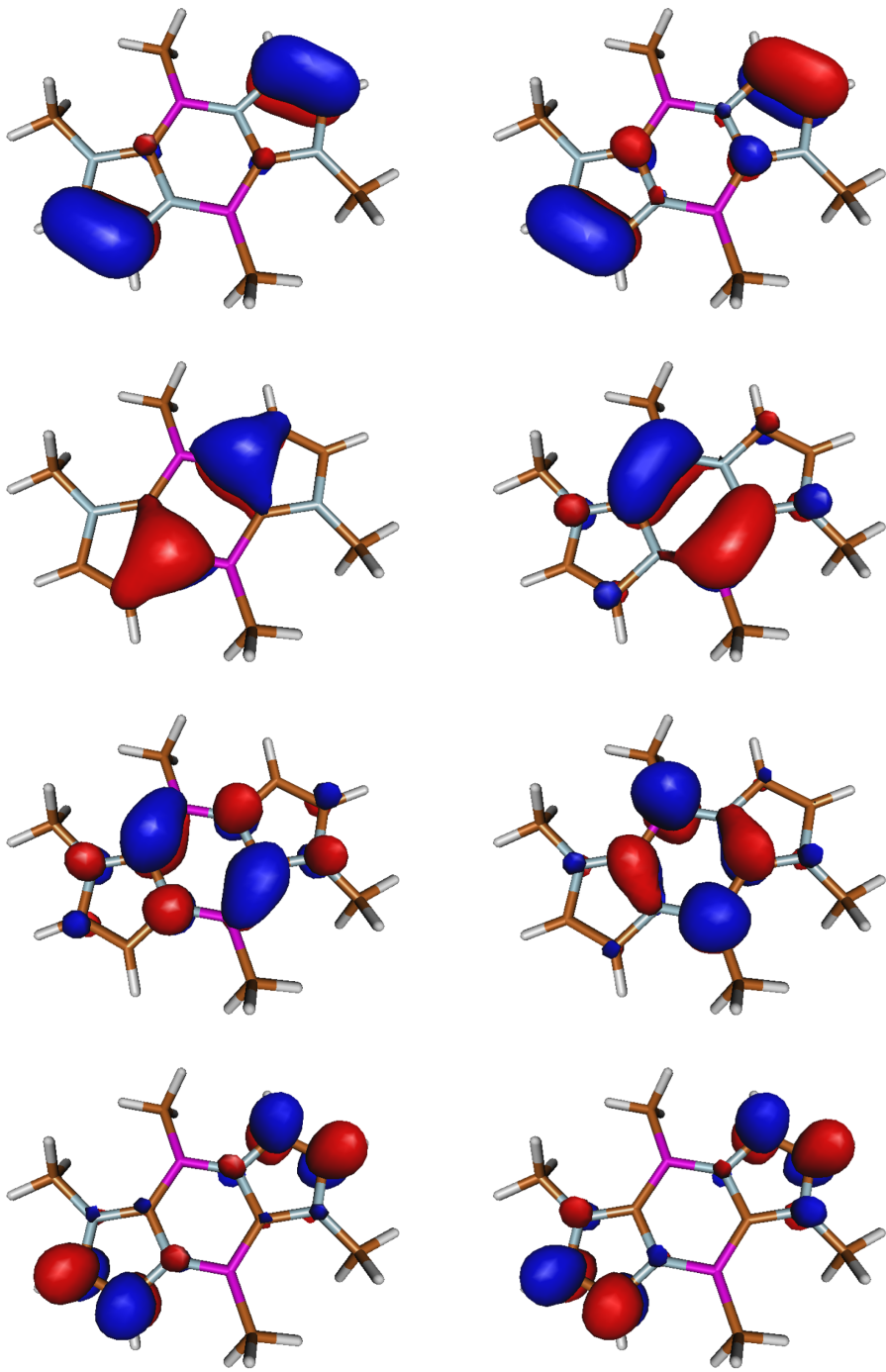


Figure S2: Active orbitals of the S_0 state of fragment A. Active orbitals of all other states in all three fragments are similar.

4 Magnetic coupling in organic radicals

4.1 Computational information

The calculations based on Density Functional Theory (DFT), Difference Dedicated Configuration Interaction⁹ (DDCI) and N-Electron Valence state Perturbation Theory¹⁰ (NEVPT2) were performed with the Orca 4.2 code.² DFT calculations were performed using the unrestricted B3LYP exchange-correlation hybrid functional.^{11,12} In the DFT calculations, the magnetic coupling constant, J_{AB} , has been computed from the energy of the triplet (high-spin, HS) and broken symmetry (BS) states by applying the so-called Yamaguchi formula to correct for spin contamination:¹³

$$J_{AB} = \frac{2(E_{BS} - E_{HS})}{\langle \hat{S}^2 \rangle_{HS} - \langle \hat{S}^2 \rangle_{BS}} \quad (5)$$

based on the Heisenberg Hamiltonian written as

$$\hat{H} = -J_{AB}\hat{S}_A \cdot \hat{S}_B \quad (6)$$

Gaussian type basis sets of triple- ζ + polarisation quality¹⁴ (def2-TZVP) were applied for all atoms in the B3LYP and CASSCF/NEVPT2 calculations. A smaller basis set of split valence plus polarisation quality¹⁴ (def2-SVP) was employed in the DDCI calculations. Test DDCI calculations with a def2-TZVP basis set lead to similar results but at much larger computational cost. The threshold for selecting the configurations external to the CAS was set to 10^{-9} . This is the largest threshold for which the effect of the determinants with smaller coefficients (estimated with second-order perturbation theory) becomes negligible.

The complete active space second-order perturbation theory (CASPT2) calculations were performed with OpenMolcas.¹ ANO-RCC basis sets¹⁵ with a (5s,4p,2d,1f) contraction for C and N atoms, (6s,5p,2d,1f) for S and (3s,2p,1d) for H, were applied. All electrons were included in the perturbational treatment of the dynamic correlation except the deep-core electrons (1s²,2s²,2p⁶ for S, and 1s² for C and N). These basis sets were also employed in the computation of the CASSCF wave functions of the monomers used to construct the MEBFs for the NOCI calculations.

The threshold for the construction of the common MO basis to express the two-electron integrals was set to 10^{-5} .

Table S12: Cartesian coordinates (in Å) of the B3LYP/def2-TZVP 4-NCBTA structure.

Atom	x	y	z
C	-0.700740	0.000000	0.000000
C	0.700740	0.000000	0.000000
C	1.411538	1.198405	0.000000
C	0.714837	2.402253	0.000000
C	-0.674474	2.418459	0.000000
C	-1.397280	1.219577	0.000000
H	2.493904	1.191863	0.000000
H	1.260727	3.336232	0.000000
H	-1.214978	3.355038	0.000000
S	1.384096	-1.613421	0.000000
S	-1.400891	-1.601628	0.000000
N	-0.011623	-2.502181	0.000000
C	-2.824645	1.234953	0.000000
N	-3.977850	1.237893	0.000000

4.2 Spin density and Mulliken spin populations of 4-NCBDA

Table S13: Mulliken atomic spin populations of the CASSCF(3,3) and CASSCF(5,5) doublet wave functions of the ground state of 4-NCBDA. The populations on the three hydrogen atoms are smaller than 0.001 in all cases.

Atom	C1	C2	C3	C4	C5	C6	C7	S1	S2	N1	N2
CAS(3,3)	0.004	0.005	0.006	0.004	0.005	0.005	0.000	0.139	0.134	0.698	0.000
CAS(5,5)	0.004	0.005	0.006	0.004	0.005	0.005	0.000	0.140	0.134	0.697	0.000

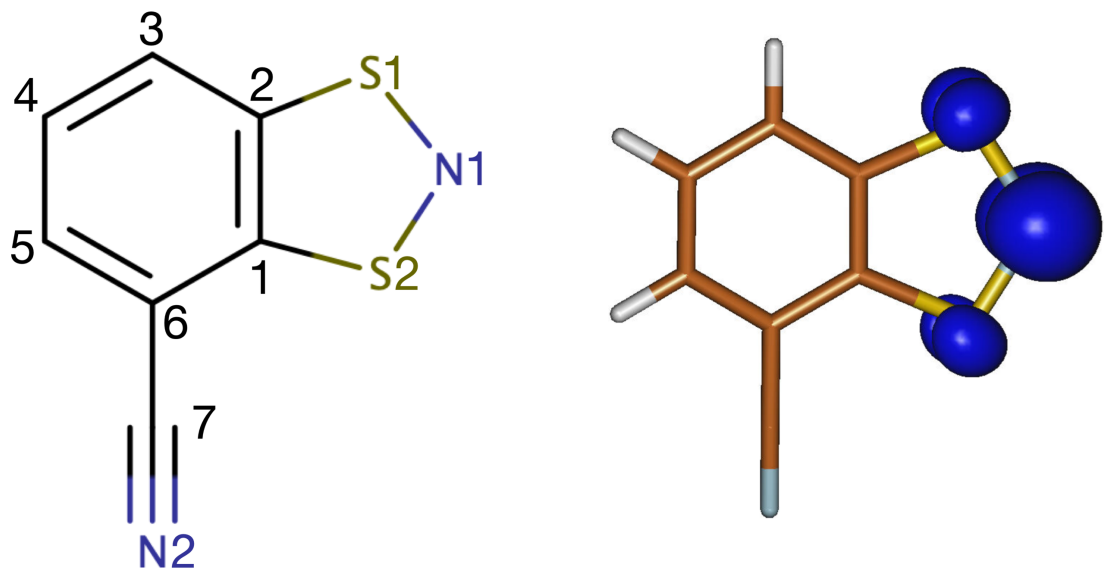


Figure S3: Atom numbering as used in Table S11 (left) and CASSCF(3,3) spin density plot (right). The plot of the CASSCF(5,5) is indistinguishable from the plot here depicted.

4.3 Threshold for selection of determinant pairs in NOCI-F

Figure S4 shows the convergence of the calculated coupling parameter with the threshold τ_{CI} to select determinants pairs in the calculation of the NOCI matrix elements. The curves show that either using fragment wave function obtained from a CAS(3,3) or CAS(5,5) converge to the same magnetic coupling parameter. The convergence is much faster with the smaller CAS wave functions; for the CAS(3+3,3+3) MEBFs small changes are observed for $\tau_{CI} \leq 10^{-4}$, while one has to go three orders of magnitude smaller for the CAS(5+5,5+5) MEBFs. The number of determinants pairs considered in the calculation of the matrix elements increases rapidly with smaller τ_{CI} as shown in Fig. S5. For the smaller CAS wave functions, the number of pairs is around 1000 for converged results. The larger CAS requires at least $5 \cdot 10^6$ determinant pairs to obtain reliable couplings. Finally, Fig. S7 illustrates that the trend of J_{AB} versus τ_{CI} is the same in all the geometries that we have studied. Notice that there are less data points in this figure than in Fig. S4, which explains the apparently different shape of the curve for the dimer in the experimental geometry.

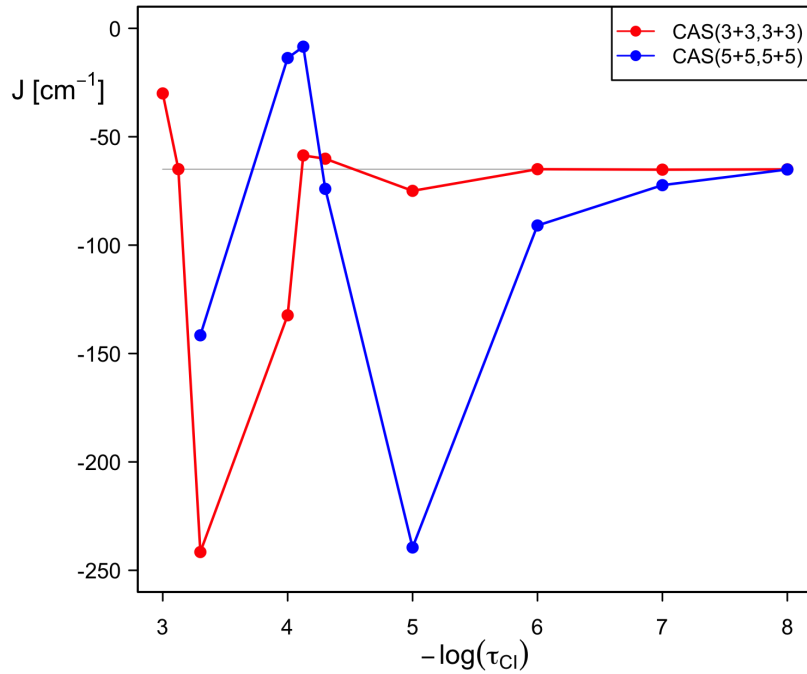


Figure S4: Magnetic coupling parameter J_{AB} between two 4-NCBTA radicals extracted from the 300 K experimental structure as function of τ_{CI} , the threshold for including determinant pairs in the calculation of the NOCI matrix elements.

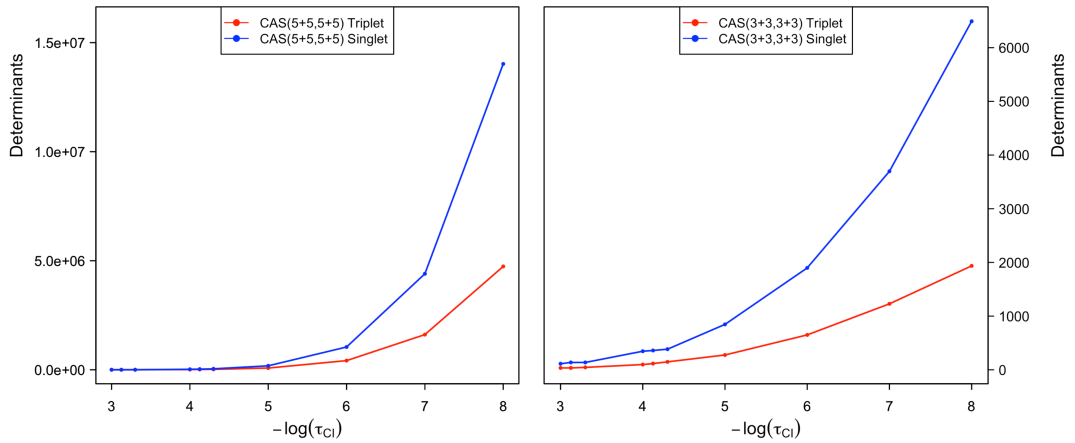


Figure S5: Number of determinant pairs in the calculation of the $\langle S_0 S_0 | \hat{H} | S_0 S_0 \rangle$ and $\langle T_0 T_0 | \hat{H} | T_0 T_0 \rangle$ elements of the NOCI matrix as function of τ_{CI} , the threshold for selecting determinant pairs.

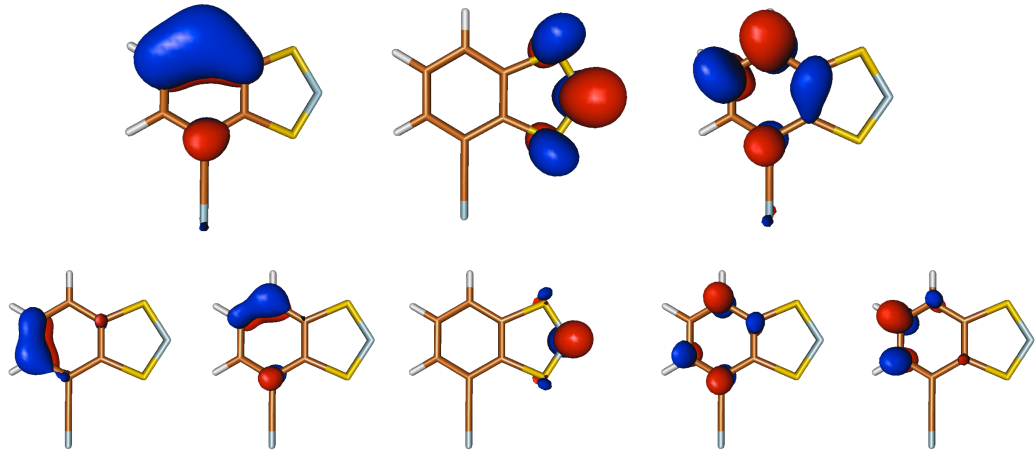


Figure S6: CASSCF(3,3) (up) and CASSCF(5,5) (down) active orbitals of the 4-NCBTA radical used to calculate the fragment wave functions in NOCI-F.

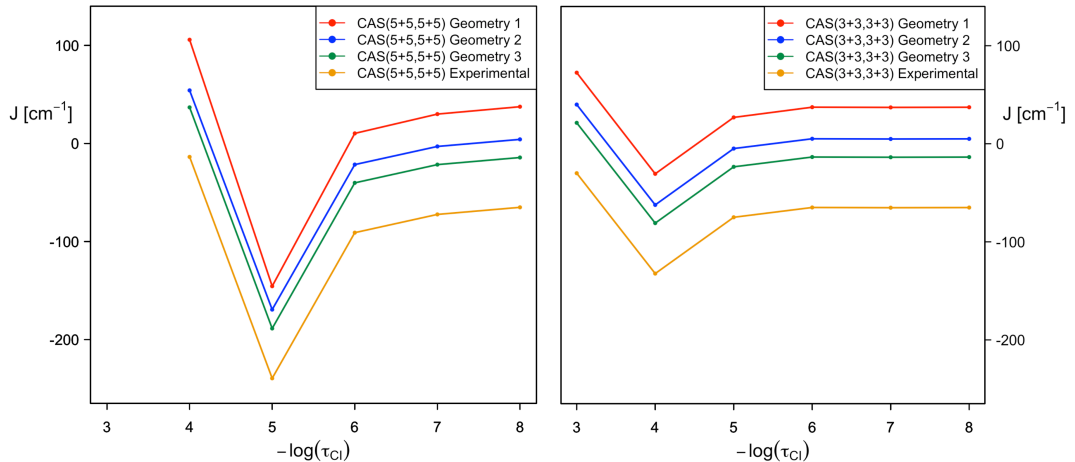


Figure S7: Magnetic coupling parameter J_{AB} between two 4-NCBTA radicals at four different relative orientations as function of τ_{CI} , the threshold for including determinant pairs in the calculation of the NOCI matrix elements.

4.4 Comparison of different computational approaches

Table S14: Magnetic coupling parameter J_{AB} (in cm^{-1}) between selected 4-NCBTA radical pairs calculated by various computational approaches.

	geometry 1	geometry 2	geometry 3	HT(300 K)	LT(180 K)
B3LYP	193	-92	-360	-655	-3476
CASSCF(6,6)	82	3	-39	-160	-1815
CASSCF(10,10)	70	3	-38	-153	-1760
CASSCF(6,6) + CASPT2(0.25)	431	-648	-703	-956	-4628
CASSCF(10,10) + CASPT2(0.25)	453	-590	-641	-922	-4552
CASSCF(6,6) + CASPT2(0)	1096	-108	-319	-623	-3822
CASSCF(10,10) + CASPT2(0)	1122	-82	-270	-564	-3766
CASSCF(6,6) + NEVPT2	1147	-40	-243	-552	-4109
CASSCF(10,10) + NEVPT2	1106	-45	-248	-520	-4004
DDCI on CAS(2,2)	289	-30	-153	-317	-2298
NOCH-F CAS(3,3) + DCEC					
GS + CT + excited doublets + CASPT2(0.25)	240	-22	-144	-353 (-362)	-2780 (-2789)
GS + CT + excited doublets + CASPT2(0)	250	-14	-113	-290 (-295)	-2388 (-2366)

4.5 Magnetic coupling for PDTA

Following the conclusions of the 4-NCBDA study, the MEBFs of the NOCI-F are constructed from the CASSCF(3,3) fragment wave functions. Dynamic correlation shifts correspond to the CASPT2(0) correction of the CASSCF(11,11) results of the fragments. The reference wave function for the NEVPT2 and CASPT2 calculations of the dimer has 10 electron distributed in 10 orbitals. Graphical representations of these orbitals are given in Fig. S8.

A comparison of the NOCI-F magnetic coupling with and without dynamic correlation shift is given in Fig. S9. The NOCI-F results without dynamic correlation correction underestimated the ferromagnetic character in the interval shown in the figure. Applying the shift calculated with CASSCF(3,3)/CASPT2(0) brings J in close to the DDCI reference values and the correction extracted from CASSCF(11,11)/CASPT2 calculations results in even better agreement. Corrections based on CASPT2(0.25) lead to less accurate couplings.

Table S15: Cartesian coordinates (in Å) of the PDTA structure.

Atom	x	y	z
C	-0.69748	-1.58713	0.00000
C	0.69748	-1.58713	0.00000
C	0.71206	0.67657	0.00000
C	-0.71206	0.67657	0.00000
N	1.42279	-0.44820	0.00000
N	-1.42279	-0.44820	0.00000
N	0.00000	3.19151	0.00000
H	-1.26031	-2.52298	0.00000
H	1.26031	-2.52298	0.00000
S	-1.40117	2.28598	0.00000
S	1.40117	2.28598	0.00000

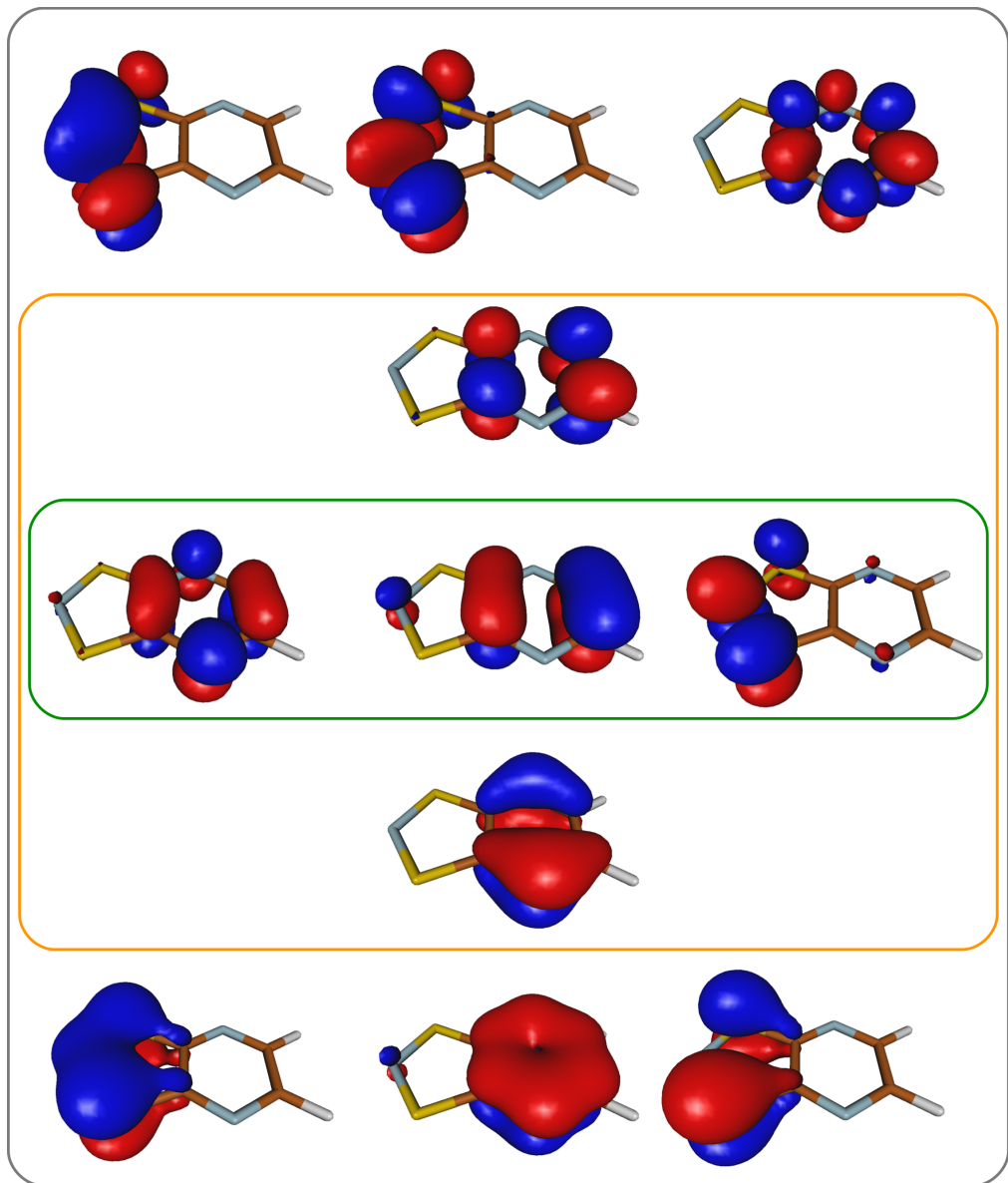


Figure S8: Active orbitals of the PDTA radical. The three orbitals inside the green box in the middle are used in the $\text{CAS}(3,3)$ calculations to construct the fragment wave function for the NOCI MEBFs; plus and minus combinations on a pair of radicals of the five orbitals in the orange box span the $\text{CAS}(10,10)$ of the dimers; and the 11 orbitals in the grey box are used in the CASPT2 calculation to calculate the dynamic correlation shift for NOCI-F.

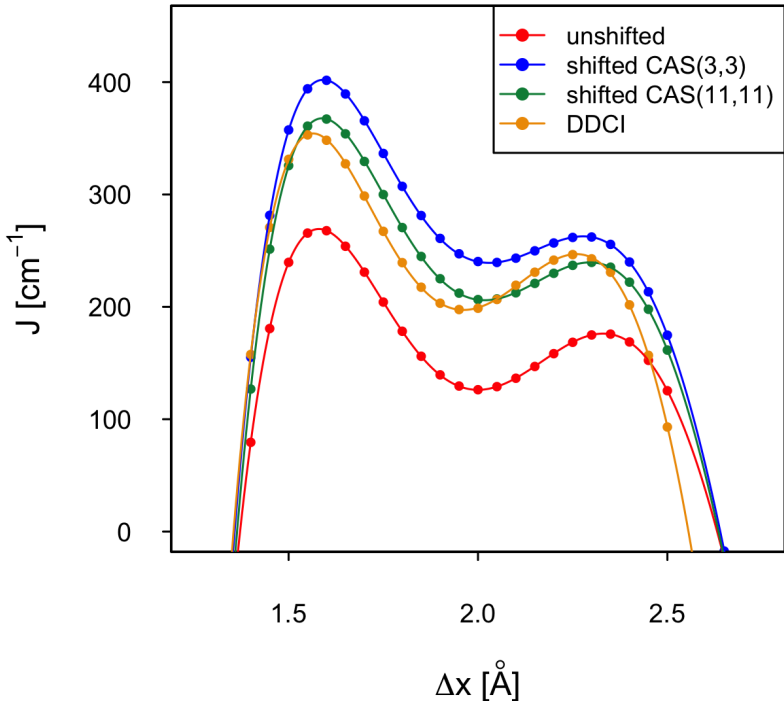


Figure S9: NOCI-F and DDCI magnetic coupling strength of the PDTA dimer as function of the slippage Δx

Figure S9 compares the magnetic coupling parameters calculated with NOCI-F using no dynamic correlation, the CASSCF(3,3)/CASPT2, or the CASSCF(11,11)/CASPT2 shift to the DDCI results. The unshifted NOCI-F results reproduce very accurately the DDCI trend but slightly underestimate the ferromagnetic character. The application of the dynamic correlation correction from CASSCF(3,3)/CASPT2 calculations on the fragments leads to an almost quantitative agreement, which is slightly improved when the CASSCF(11,11)/CASPT2(0) correction is applied.

4.6 DDCI versus NOCI-F: timings

The DDCI/def2-svp calculations were performed with Orca and required rather stringent thresholds to converge to a stable J_{AB} . The calculations for PDTA with $t_{sel} = 10^{-9}$ took approximately 36 minutes on a workstation with 2 EPYC 7282 CPUs (2x16 cores), this increased to 1 hour 10 minutes when t_{sel} is reduced to 10^{-9} . Calculations with a larger basis set (def2-tzvp) could only be done with $t_{sel} = 10^{-6}$ (giving practically the same results as with the def2-svp basis applying the same threshold), and took more than 13 hours. The NOCI calculations are much less dependent on the basis set as one only has to consider the monomers in the AO basis, dimers are treated in the much smaller common MO basis. The NOCI calculation (not counting the preparation of the CASSCF fragment wave functions and the dynamic correlation correction) took 16 minutes on a small workstations with two V100 GPUs and two Xeon Silver 4214 CPUs. Each GPU handled three ranks applying the MPS protocol, the CPUs were used for the singular value decompositions and the eigenvalue solvers. The preparation phase takes less than 15 minutes.

References

- [1] F. Aquilante, J. Autschbach, A. Baiardi, S. Battaglia, A. C. Borin, L. Chibotaru, I. Conti, L. De Vico, M. Delcey, I. Fernández-Galván, N. Ferré, L. Freitag, M. Garavelli, X. Gong, S. Knecht, E. D. Larsson, R. Lindh, M. Lundberg, P.-Å. Malmqvist, A. Nenov, J. Norell, M. Odelius, M. Olivucci, T. B. Pedersen, L. Pedraza-González, Q. M. Phung, K. Pierloot, M. Reiher, I. Schapiro, J. Segarra-Martí, F. Segatta, L. Seijo, S. Sen, D.-C. Sergentu, C. J. Stein, L. Ungur, M. Vacher, A. Valentini, and V. Veryazov. Modern quantum chemistry with [Open]Molcas. *J. Chem. Phys.*, 152:214117, 2020.
- [2] F. Neese, F. Wennmohs, U. Becker, and C. Riplinger. The ORCA quantum chemistry program package. *J. Chem. Phys.*, 152:224108, 2020.
- [3] R. Dovesi, A. Erba, R. Orlando, C. M. Zicovich-Wilson, B. Civalleri, L. Maschio, M. Réat, S. Casassa, J. Baima, S. Salustro, and B. Kirtman. Quantum-mechanical condensed matter simulations with CRYSTAL. *WIREs Comput. Mol. Sci.*, 8:e1360, 2018.
- [4] S. Grimme, A. Hansen, J. G. Brandenburg, and C. Bannwarth. Dispersion-corrected mean-field electronic structure methods. *Chem. Rev.*, 116:5105–5154, 2016.
- [5] B. Wang, Y. Li, R. Ganguly, H. Hirao, and R. Kinjo. Ambiphilic boron in 1,4,2,5-diazadiborinine. *Nature Comm.*, 7:11871, 2016.
- [6] D. Vilela Oliveira, J. Laun, M. F. Peintinger, and T. Bredow. BSSE-correction scheme for consistent gaussian basis sets of double- and triple-zeta valence with polarization quality for solid-state calculations. *J. Comput. Chem.*, 40:2364–2376, 2019.
- [7] H. J. Monkhorst. Special points for Brillouin-zone integrations. *Phys. Rev. B*, 13:5188–5192, 1976.
- [8] J. D. Pack and H. J. Monkhorst. "special points for Brillouin-zone integrations" –a reply. *Phys. Rev. B*, 16:1748–1749, 1977.
- [9] J. Miralles, J.-P. Daudey, and R. Caballol. Variational calculation of small energy differences. the singlet-triplet in $[\text{Cu}_2\text{Cl}_6]^{2-}$. *Chem. Phys. Lett.*, 198(6):555–562, 1992.

- [10] C. Angeli, R. Cimiraglia, S. Evangelisti, T. Leininger, and J.-P. Malrieu. Introduction of n-electron valence states for multireference perturbation theory. *J. Chem. Phys.*, 114:10252–10264, 2001.
- [11] A. D. Becke. Density-functional thermochemistry. III. The role of exact exchange. *J. Chem. Phys.*, 98(7):5648–5652, 1993.
- [12] C. Lee, W. Yang, and R. G. Parr. Development of the colle-salvetti correlation-energy formula into a functional of the electron density. *Phys. Rev. B*, 37:785, 1988.
- [13] K. Yamaguchi, H. Fukui, and T. Fueno. Molecular orbital (MO) theory for magnetically interacting organic compounds. Ab-initio MO calculations of the effective exchange integrals for cyclophane-type carbene dimers. *Chem. Lett.*, 15:625–628, 1986.
- [14] F. Weigend and R. Ahlrichs. Balanced basis sets of split valence, triple zeta valence and quadruple zeta valence quality for H to Rn: Design and assessment of accuracy. *Phys. Chem. Chem. Phys.*, 7:3297–3305, 2005.
- [15] B. O. Roos, R. Lindh, P.-Å. Malmqvist, V. Veryazov, and P.-O. Widmark. Main group atoms and dimers studied with a new relativistic ANO basis set. *J. Phys. Chem. A*, 108:2851–2858, 2004.